Lab on a Chip

A vacuum-assisted, highly parallelized microfluidic array for performing multi-step digital assays

Journal:	*Lab on a Chip*
Manuscript ID	LC-ART-07-2021-000636.R1
Article Type:	Paper
Date Submitted by the Author:	02-Oct-2021
Complete List of Authors:	Hu, Jiumei; Johns Hopkins University, Mechanical Engineering Chen, Liben; Johns Hopkins University, Mechanical Engineering Zhang, Pengfei; Johns Hopkins University, Biomedical Engineering Hsieh, Kuangwen; Johns Hopkins University, Department of Mechanical Engineering Li, Hui; Johns Hopkins University, Mechanical Engineering Yang, Samuel; Stanford University, Department of Emergency Medicine Wang, Jeff; Johns Hopkins University, Mechanical Engineering

A vacuum-assisted, highly parallelized microfluidic array for performing multi-step digital assays

Jiumei Hu[1], Liben Chen[1, *], Pengfei Zhang[2], Kuangwen Hsieh[1], Hui Li[1], Samuel Yang[3] and Tza-Huei Wang[1, 2, 4,*]

[1]Department of Mechanical Engineering, Johns Hopkins University, Baltimore, Maryland 21218, United States

[2]Department of Biomedical Engineering, Johns Hopkins School of Medicine, Baltimore, Maryland 21205, United States

[3] Department of Emergency Medicine, Stanford University, Stanford, California, United States

[4]Institute for NanoBiotechnology, Johns Hopkins University, Baltimore, Maryland 21218, Unites States

*Corresponding authors: Email: lchen@jhu.edu and thwang@jhu.edu, Tel: (+1) 410-516-7086

Abstract

There remains an unmet need for a simple microfluidic platform that can perform multi-step and multi-reagent biochemical assays in parallel for high-throughput detection and analysis of single molecules and single cells. In response, we report herein a PDMS-based vacuum-driven microfluidic array that is capable of multi-step sample loading and digitalization. The array features multi-level bifurcation microchannels connecting to 4096 dead-end microchambers for partitioning liquid reagents/samples. To realize multi-step repetitive liquid sample loading, we attach an external vacuum onto the chip to create internal negative pressure for a continuous liquid driving force. We demonstrated a high uniformity of our device for three sequential liquid loadings. To further improve its utility, we developed a thermosetting-oil covering method to prevent evaporation for assays that require high temperatures. We successfully performed digital PCR assays on our device, demonstrating the efficient multi-step reagent handling and the effective anti-evaporation design for thermal cycling. Furthermore, we performed a digital PCR detection for single-cell methicillin-resistant *Staphylococcus aureus* using a three-step loading approach and achieved accurate single-cell quantification. Taken together, we have demonstrated that our vacuum-driven microfluidic array is capable of multi-step sample digitalization at high throughput for single-molecule and single-cell analyses.

Keywords: Microfluidic; Multi-step loading; Single-cell; Digital PCR; High throughput

1. Introduction

The prompt advancement of microfluidic-based digital assay platforms (e.g., digital polymerase chain reaction (dPCR)[1] and digital enzyme-linked immunosorbent assays (dELISA)[2]) has revolutionized the conventional approaches for single-cell and single-molecule analyses with much higher sensitivity and throughput. In these microfluidic platforms, numerous single cells or single molecules can be compartmentalized into discrete partitions and generate binary readouts of “0” and “1” for absolute quantification. Observation of the emerging platforms leads to two major categories based on the compartmentalization methods. The first type is the droplet microfluidics, in which aqueous solution is discretized into hundreds of thousands of water-in-oil emulsions[3, 4], whereas the second approach employs microfluidic arrays to physically isolate picoliter to nanoliter-sized liquid for digitalization[5, 6]. These two methods have been widely used for many different digital assays. Unfortunately, both of them are limited in one-step reactions, where all the samples/reagents are mixed off-chip and loaded into microfluidic devices for single-step reaction without allowing additional samples/reagents to be added afterwards. However, many biochemical assays require multi-step and multi-reagent additions. For instance, single-cell reverse transcription polymerase chain reaction (RT-PCR) requires multi-step loadings of lysis buffer, RT and PCR reagents into digital compartments for transcriptional analyses[7]. Therefore, microfluidic platforms that can perform highly parallelized digital assays with a capability of multi-step and multi-reagent processing will greatly expand the application scope of current digital assay technologies.

Toward this end, many efforts have been made for the development of microfluidic digital assay platforms that can perform multi-reagent additions and multi-step reactions. For instance, SlipChip takes advantage of the Laplace pressure difference created by non-equal dimensions between adjacent droplet confinements to load multiple sample/reagents and uses manual sliding of the device to perform multiple reactions[8]. Printing-based platfroms, such as Sequential Operation of Droplet Array (SODA), can achieve multi-step and multi-reagent assays in thousands of nanoliter-to-picoliter droplets by integrating capillary and automated mechanical translation stages for droplet deposition and reagents addition[9]. Additionally, the multiphase continuous flow droplet microfluidic systems, which merge pair-wise droplets using electrodes, can realize multi-step biochemical assays at high throughput with tens of thousands of single cells/molecules being analyzed per run[10-12]. However, these techniques are constrained either by limited analytical throughput or high engineering complexity. For example, SlipChip is limited to fifty parallel reactions[8], whereas SODA suffers from the complex engineering system[13]. For pairwise droplet merging, various parameters, such as droplet size, channel dimension, and voltage must be well-optimized to maximize the success rate of droplet fusion and the stability of fused microdroplets, thus increasing the complexity for the overall experimental design[12]. Therefore, it remains an unmet need for a facile microfluidic platform that is capable of multi-step, multi-reagent biochemical assays to analyze thousands of parallel reactions at a time.

In response, we developed an easy-to-use, high-density microfluidic device for performing multi-step, multi-reagent assays. The device is an outlet-free microarray[14, 15] containing multi-level bifurcated microchannels and 4096 dead-end microchambers, which allow for implementing thousands of parallel reactions at a time. The device utilizes a vacuum-assisted loading mechanism facilitated by gas permeability of PDMS[16-18]. To facilitate the multi-step loading, we designed a reversibly bonded suction layer that was connected to an external vacuum to create a continuous negative pressure for the microarray. Multiple liquid samples/reagents can be introduced into the device sequentially until all the microchambers are filled. To prevent evaporation at high temperatures, we used a unique thermosetting oil-poured glass coverslip to seal the top of the gas-permeable PDMS. We showcased the simplicity of the workflow and demonstrated the high uniformity of three loadings. We also performed a bacterial quantification via a single-cell digital assay with three consecutive loading steps for single-cell distribution, cell

lysis, and PCR buffer digitization and proved that single bacterial cells can be reliably detected and precisely quantified.

2. Materials and Methods

2.1 Materials and reagents

Methicillin-resistant *Staphylococcus aureus* (ATCC BAA-44, Manassas, VA) and Methicillin-sensitive *Staphylococcus aureus* (ATCC29263, Manassas, VA) bacteria strains were cultured on Tryptic Soy Agar (TSA) plates in 37 °C incubator overnight and continuously passaged every 24 h. The concentration of *S. aureus* was determined via a Nanodrop spectrophotometer (Thermo Fisher Scientific, MA, USA) and plate counting (See ***Supplementary information*** for more details).

Reagents including 2 × Taqman Gene Expression Master Mix, Tween-20, Nucleic-free water, and ChargeSwitch™ gDNA Mini Bacteria Kit used for *Neisseria gonorrhoeae* genomic DNA extraction were purchased from Thermo Fisher Scientific (Waltham, MA, USA). Bovine Serum Albumin (BSA, 20 mg/mL) was purchased from New England Biolabs Inc (Ipswich, MA, USA). Lysostaphin was purchased from Sigma Aldrich (St. Louis, MO, USA) and dissolved in a buffer of 0.05 M Tris-HCl and 0.145 M NaCl at pH 7.4 to generate 1 mg/mL stock solution. Primers and probes for *RecA* and *MecA* genes, as well as synthetic *RecA* DNA, were synthesized by Integrated DNA Technologies Inc. (Coralville, IA, USA). Sequences for all the nucleic acid products are summarized in ***Table S1***.

2.2 Device fabrication

Two reusable master molds, one with a microarray pattern and the other one with a pattern for suction layer, were prepared using the standard photolithography technique (***Fig. S1***). Photomasks were designed using AutoCAD software and printed by CAD/Art Services, Inc. (Bandon, OR, USA). Using these photomasks, SU8 micropatterns for the microarray layer and the suction layer were generated on two 4-inch silicon wafers. Based on the soft lithography technique, the multilayer PDMS device was fabricated using the SYLGARD 184 Silicone Elastomer Kit (Dow Corning, Midland, MI). Specifically, our device was assembled by four layers including the suction layer, a ~100-μm-thick PDMS membrane, the microarray layer, and a glass coverslip (***Fig. S1***). Detailed procedures for the device fabrication are provided in ***Supplementary information***.

2.3 Digital PCR and single-cell digital assay

For digital PCR amplification that targets *RecA* gene using extracted bacteria DNA or synthetic DNA fragments, the 10-μL PCR reaction mixture consisted of 5 μL of 2 × Taqman Gene Expression Master Mix, 2 μL DNA template, 0.9 μL forward primer (900 nM), 0.9 μL reverse primer (900 nM), 0.25 μL probe (250 nM), 0.1 μL of 10% tween-20 (0.1 %), 0.5 μL of 20 mg/mL BSA (1 mg/mL) and 0.35 μL nuclease-free water.

For the 3-step single bacteria detection targeting *MecA* gene, the whole reaction system was composed of 2 μL single-cell suspension, 2 μL Lysostaphin, and 8 μL PCR reaction mixture that were loaded at consecutive steps. Specifically, 10 μL of PCR reaction mixture was prepared every time before use with exactly the same proportion of each reagent as mentioned above except that we used different primer pair and probe. Then 8 μL PCR reaction mixture was aspirated and loaded into the chip at the third step for amplification. The thermocycling program for both digital PCR and single *S.aureus* detection is as follows: 50 °C for 2 min, 95°C for 10 min, 10 s at 95 °C and 60 s at 60 °C for 60 cycles.

2.4 Data acquisition and analysis

For the characterization of loading uniformity, images of full-view fluorescent chips were acquired by our in-house developed imaging platform, which is composes of a commercial flatbed heater (Bulldog Bio), a Sony 12M pixel CMOS MIL camera with a emission filter (510-550 nm, Omega Optical) and 50-mm macro focusing lens (Canon), a blue LED array (Thorlabs) with excitation filter (457-492 nm, Omega Optical) for illumination, and an Aduino to control the LED[19]. We then adopted an automated image processing program applied to chip-based digital assays for downstream data analysis[20]. Using this program, images were tilt-corrected, and each microchambers are precisely located by peak finding based on the regular structure of microarray (64 rows × 64 columns). The pixel intensity of each microchamber is then extracted, and the results are exported into a 64 × 64 Excel table for data analysis, where each value in the table corresponds to the position of each microchamber in the chip array (***Fig. S2***). All the digital PCR images were also captured on our imaging platform. We used ImageJ to count the number of positive signals. For single Methicillin-resistant *S. aureus* on-chip detection, 16 images were captured per chip under 1 × lens using the ZEISS Axio Zoom V16 microscope. Then we used ImageJ to stitch images and counted positive microchambers on the stitched picture for statistical analysis.

3. Results and Discussions

3.1 Device design and working principle

Our device consists of a suction layer, a thin PDMS membrane layer, a microarray layer, and a glass coverslip (***Fig. 1A***). The suction layer features a cavity that is connected to an external vacuum and cylindrical micropillars that prevent cavity collapse due to vacuum. The size of the micropillar is 150 μm in diameter and 100 μm in height, with spacing between each micropillar as 250 μm. The ~100-μm-thick PDMS membrane was fabricated by our ultrathin layering technique[19] to ensure efficient gas permeation under vacuum while also maintain sufficient toughness of the film. The microarray layer is composed of 12-level bifurcated microchannels and 4096 (2^{12}) dead-end microchambers (64 rows × 64 columns). To maximize liquid transport efficiency with minimal energy cost, we followed Murray's Law[21] and designed the length and width ratio between mother and daughter branches to be 0.7937 and 0.7071, respectively, with a channel height of 100 μm. The dimension of each dead-end microchamber is 180 μm × 100 μm × 200 μm (length × width × height), which can hold ~3.5 nL in volume. The microarray, therefore, has the capacity to analyze up to 14 μL of samples. During chip assembly, the patterned side of the microarray layer was facing up to bond with the thin PDMS membrane, and the other side was plasma bonded with a clean glass coverslip to provide a solid support for the whole device.

Our device achieves multi-step, simultaneous sample loading into thousands of nanoliter-sized microchambers by leveraging the gas permeability of PDMS. At the peripheral area of the suction layer, four pneumatic ports (***Fig. 1B***) are connected to the house vacuum via four Tygon microbore tubings (inner dimameter = 0.02 inches) inserted with blunt needles (22 guage). We then open the vacuum valve to provide continuous, uniform vacuum across the whole device. The air inside of the microarray layer diffuses through the thin PDMS membrane upon vacuum applied, creating an imbalanced pressure between the atmosphere and the microarray that initiates vacuum-driven sample digitalization. Importantly, the tree-like multi-level bifurcation microchannel is designed to split liquid at each junction so that all aliquoted liquids can simultaneously arrive at thousands of dead-end microchambers. Moreover, the thick suction layer serves as a continuous "vacuum battery" until the loading is done. To achieve multi-step, multi-reagent loading, we can control the loading volume of each step/reagent so that each microchamber is only partially filled until the whole microchambers are fully occupied (***Fig. 1C***).

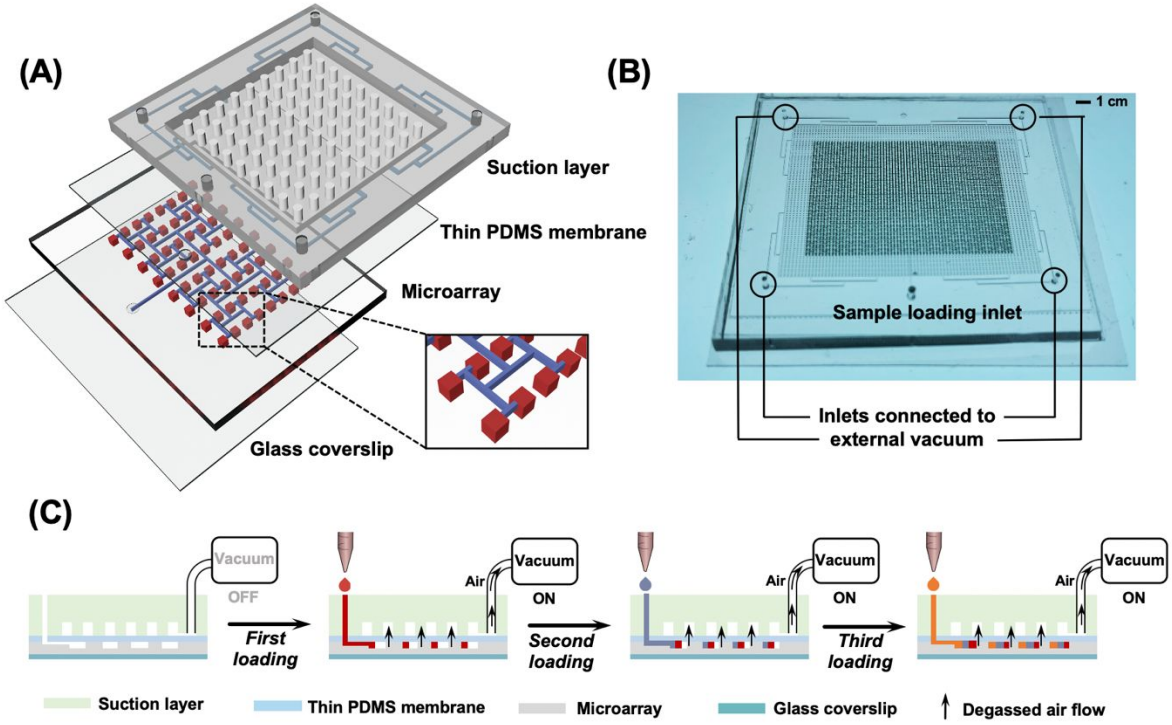

Fig. 1. Chip design and working principle of multi-step sample loading. (A) Our multi-layer PDMS device is fabricated by assembling a suction layer, a thin PDMS membrane, a microarray layer, and a glass coverslip. The suction layer features a large cavity with a micropillar array to prevent the cavity from collapsing. The microarray is composed of 12-level bifurcated channels and 4096 dead-end microchambers. (B) Four inlets on the suction layer are connected to an external vacuum to create a long-term negative pressure within the microarray and therefore facilitate the sample loading process. The size of our device is ~45 mm × 40 mm. Scale bar: 1 cm. (C) Based on the multi-level bifurcation structure of the microarray, multi-step and multi-reagent loading is achieved by introducing a fractional volume of sample into the chip in each step until all the microchambers are completely filled.

3.2 Simple and uniform multi-step loading

The vacuum-assisted multi-step loading mechanism facilitates a fast and easy operation of our device without any lengthy pre-treatments such as degasification. To this end, we first connected the four pneumatic inlets of the suction layer of a freshly fabricated device with a house vacuum for one minute to create a negative pressure within the device. To load the first reagent/sample into the microchambers, we used a regular pipette to transfer the liquid into a 10-μL pipette tip with precise volume and then inserted the tip into the inlet of the device, where the negative pressure generated by the vacuum automatically initiated the loading process. The reagent/sample first ran through 12-level bifurcated microchannels, splitted equally at each junction and then divided into 2^{12} aliquots distributing in 4096 dead-end microchambers. This same loading can be repeated multiple times (with a total volume < 14 μL) for sequentially adding multiple reagents/samples into microchambers. Finally, to completely isolate the biochemical reactions in each microchamber, we loaded partitioning oil (100-cSt silicone oil + PDMS) to seperate all the microchambers (***Video S1***). Conceretly, we preloaded the partitioning oil on top of the final sample/reagent into a pipette tip to create a tight water-oil interface, such that the oil was loaded followed by the sample/reagent without introducing any air. We found that the 100-μm channel height is necessary to ensure efficient loading of the highly viscous partitioning oil (***Supplementary information*** *and* ***Fig. S3***). With the optimal channel design, the continuous vacuum-assisted loading allows for three-step sample digitalization and oil partitioning on our device within 10 minutes.

For implementing multi-step assays on our device, multiple samples/reagents need to be loaded sequentially at different time points to initiate or regulate these parallel reactions, where uniform liquid volumes in each microchamber are necessary for accurate detections. As such, to characterize sample loading uniformity in the multiple loading steps, we used Fluorescein solution (1 μM) as a mock sample and sequentially loaded 4 μL of the solution into the chip three times. The chip was imaged after each loading step using our in-house developed imaging platform. Each image is an 8-bit RGB color image, which were converted to 8-bit grayscale. Fluorescence intensity is represented by the value of pixel, which ranges from 0 to 255. We then normalized the fluorescence intensity of each microchambers on each image by subtracting the background pixel values from the same image. The fluorescence images presented in ***Fig. 2A*** shows the accumulation of liquid in each microchambers after first, second, and third loading, respectively. Subsequently, we analyzed the fluorescence intensities of 900 microchambers on each image and plotted histograms for each loading step. As shown in ***Fig. 2B***, the fluorescence intensities of the microchambers increased after each loading step. The average intensities after first, second, and third loading are 2115, 4394, and 6550 respectively. We also calculated the Coefficient of Variations (CVs), defined as the ratio of the standard deviation to the mean, for each loading step. The CVs for the first, second, and third loading are 10.2%, 9.7%, and 9.0%, respectively. Additionally, to show the reproductivity of our device for multi-step loading, three chips were tested with three consecutive loading of Fluorescein (4 μL per loading). A linear regression (R^2=0.9895) for the normalized fluorescence intensity against the normalized sample volume indicates a reliable multiple-reagent, multi-loading assay being implemented on our device (***Fig. 2C***).

The minimal volume that can be reliably dosed into our device with uniform distribution across 4096 microchambers is ~2 μL for each loading step. Aliquots were stagnant within microchannels instead of completely flowing into microchambers when the loaded sample volume was 1.5 μL. Further decreasing the volume to 1 μL resulted in the occurrence of empty microchambers due to the ineffective liquid splitting (***Fig. S4***). We demonstrated up for six steps of uniform loading with 2 μL/step using a food dye (***Video S2***). Of note, the number of loading steps can be further scaled up by increasing the size or number of microchambers to hold a higher volume.

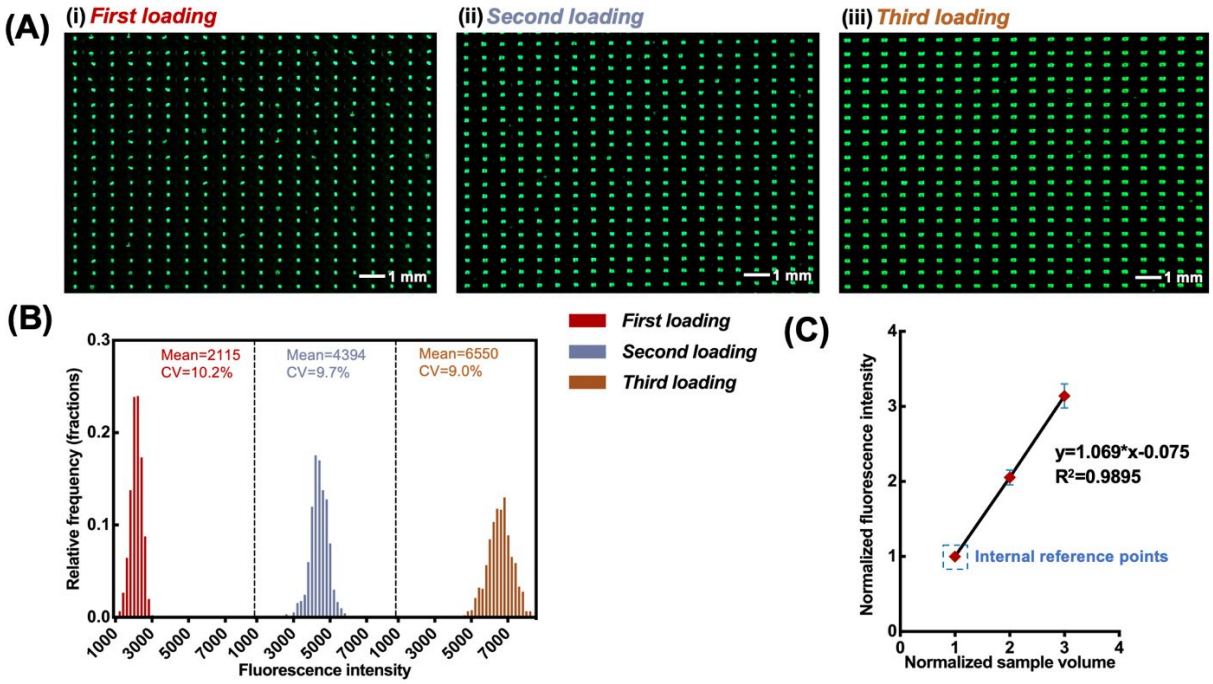

Fig. 2. Sample loading uniformity. After sequentially loaded 4 μL of Fluorescein solution 3 times, the chip was imaged on an in-house developed imaging platform. The fluorescence intensity increment of each microchamber can be clearly observed. (Ai)-(Aiii) refers to the fluorescent images after first, second, and third loading, respectively. Scale bar: 1 mm. (B) To visualize the changes of microchambers after each loading step, we plotted the frequency distribution histograms for the 900 microchambers after the first, second, and third loading. Each bar represents the fraction of observations within certain bins of values. Middle values displayed on the x-axis for each histogram proportionally increased with multiple loading steps, showing the accumulation of samples within microchambers. CVs for after each loading step is calculated and labeled above each corresponding histogram. (C) A linear regression for the normalized fluorescence intensity against the normalized sample volume was performed (n=3). A high linearity (R^2=0.9895) indicated a good reproducibility of the multi-step loading on our device.

3.3 Optimized thermosetting oil for rapid sealing and limited evaporation

Toward performing a broad range of assays that happen at different temperatures in our microarray, especially at high temperatures (e.g. PCR) where the evaporation of tiny volume can be significant, we devised a facile method that allows us to minimize sample evaporation across the entire chip for robust reactions. Following the multi-step sample loading and oil partitioning, the reversibly bonded suction layer was peeled off, leaving the thin gas-permeable PDMS membrane exposed in air. Without appropriate protection, severe evaporation of the reagents within microarray will happen at elevated temperatures. To minimize the evaporation, we used a glass coverslip to cover the PDMS membrane. The glass coverslip (45mm × 50mm) was poured with ~2 mL thermosetting oil as we were peeling off the suction layer. To cover the PDMS membrane with the glass coverslip, we slowly lay the PDMS device onto the glass to have uniform oil spreading across the top of the PDMS without introducing any bubbles (***Video S3***). The thermosetting oil, composed of 100-cSt silicone oil, 10:1 PDMS polymer, and platinum catalyst (Sigma Aldrich, St. Louis, MO), can be cured within few minutes at relatively low temperature (~50 °C) to create a firm bond between the membrane and the glass (***Fig. 3A***). The concentration of Platinum catalyst in the oil determines the curing time. We tested different thermosetting oil mixtures to optimize the Platinum catalyst concentration by using 100-cSt silicone oil and 10:1 PDMS polymer as the base components with the addition of different amounts of Platinum catalyst to create three proportions including 0.14%, 0.27%, and 0.40%. We found that the thermosetting oil with 0.27% Platinum catalyst can be cured at 50 °C in 2.5 minutes. In contrast, oil with 0.14% Platinum catalyst took relatively longer time to cure, and oil with 0.40% Platinum catalyst was

cured too fast, where curing can happen even within 10 minutes under room temperature and thus subjecting to the inconvenience for experiment operation (***Fig. 3B***). Therefore, we determined the one with 0.27% Platinum catalyst to be used as our thermosetting oil. To test the anti-evaporation performance, we compared the volume of each microchamber before and after a complete PCR thermocycling using green food dye. We did not observe any apparent evaporation (***Fig. 3C***). Furthermore, we showed that the sandwich structure (glass-PDMS-glass) can effectively prevent evaporation during PCR thermocycling by testing a digital PCR assay on the chip using genomic DNA extracted from 10^6 and 10^5 CFU/mL *Neisseria gonorrhoeae* cells (***Fig. 3D***). The strong fluorescence signals in positive microchambers showed that the digital PCR can run successfully on our device.

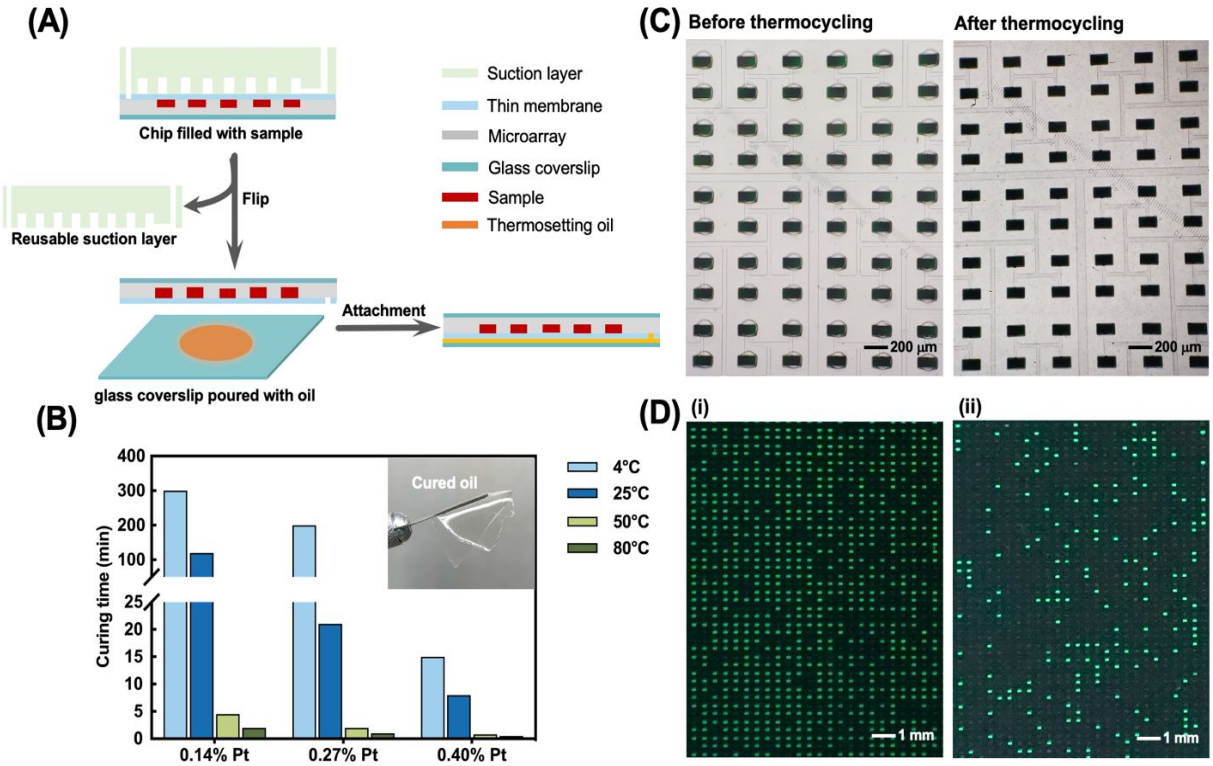

Fig. 3. Device operation and anti-evaporation performance. (A) The chip is first loaded with a sample by applying an external vacuum on the suction layer. The vacuum is then disconnected, and the suction layer is removed from the device. Next, the chip is attached to a glass coverslip coated with thermosetting oil. The assembled chip is directly put onto a flatbed PCR machine for thermocycling. Of note, the peeled suction layer is reusable as long as it remains intact and clean. (B) Thermosetting oils with different Platinum catalyst proportions are cured at various speeds and temperatures. The thermosetting oil with Pt proportion as 0.27% can stay in liquid state before heating and be cured in 2.5 minutes at 50°C. The photograph on the top right shows the cured thermosetting oil. (C) Before and after thermocycling, there were no visible differences of sample volume within each microchambers, demonstrating the good anti-evaporation performance of the sandwich structure using thermosetting oil coated glass slide. Scale bar: 200 μm. (D) A successful digital PCR assay run on the chip further proved the anti-evaporation performance of the "Sandwich-like" chip structure. The dPCR was performed using 2 μL of genomic DNA extracted from 10^6 (i) and 10^5 (ii) CFU/mL *Neisseria gonorrhoeae* cultures. Scale bar: 1mm.

3.4 Digital PCR with multi-step loading

To demonstrate that variable multi-step and multi-reagent operations can be achievable on our device and to verify these operations would not affect the performance of digital assays, we performed digital PCR using three different reagent loading methods: one-step loading (DNA target and PCR reagents were mixed and loaded into the chip altogether), two-step loading (DNA target was loaded first, followed by loading PCR reagents), and three-step loading (DNA target

was loaded first, then primers and probe were loaded, followed by loading all the other components for PCR amplification) for the detection of the same DNA target (synthetic *RecA* DNA fragment) and compared their performance. Digital PCR of each loading schemes were tested for three times. The concentration of loaded *RecA* DNA in these three loading methods was set to ~300 copies/chip. The digital PCR images for the one-step (***Fig. 4A)***, two-step (***Fig. 4B)***, and three-step (***Fig. 4C)*** approaches show no significant difference. We used the Poisson distribution methodology (See ***Supplementary information*** for details) to calculate the detected DNA copies on these digital PCR images by applying equation as follows, where N is the total number of microwells, and M is the number of positive microwells:e

$$DNA\ copy\ number = -N \times \ln\left(1 - \frac{M}{N}\right)$$

The calculated copy numbers from the number of positive microchambers after digital PCR show consistency among the three loading methods (***Fig. 4D***), demonstrating multi-step loading does not affect the ability for absolute quantification of digital PCR.

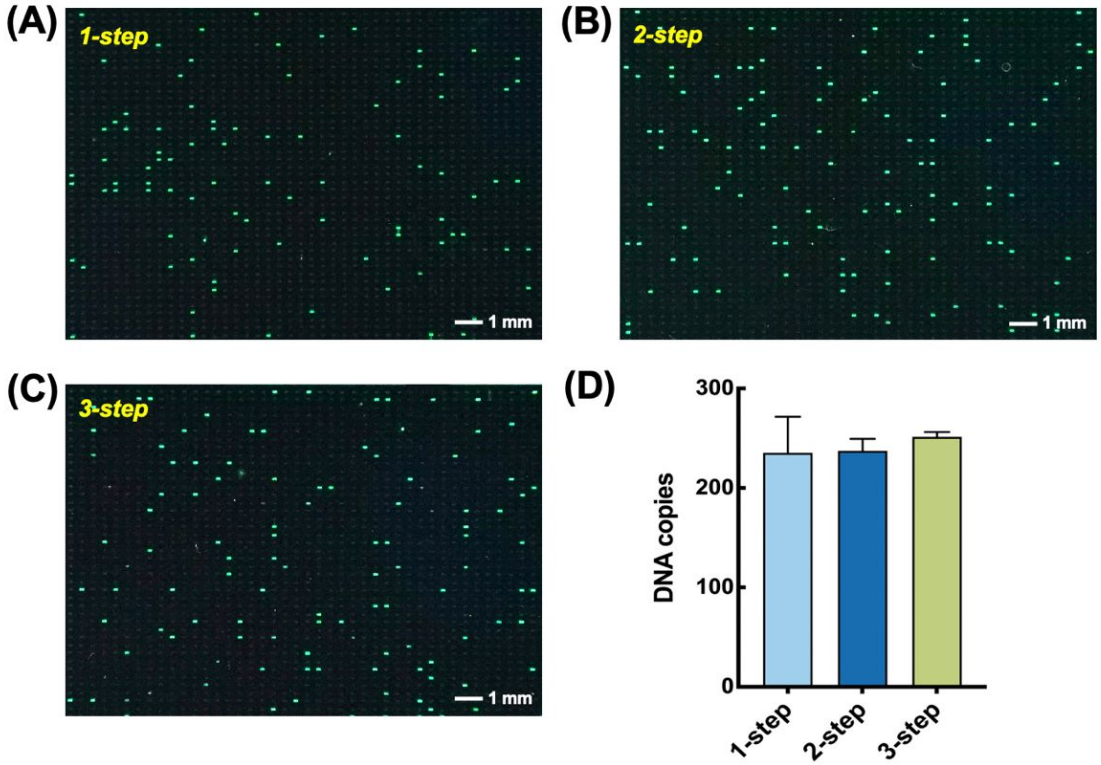

Fig. 4. Digital PCR results with different loading approaches. (A-C) To test biological assays on our multi-step loading device, we performed digital PCR reactions with one-step, two-step, and three-step loading methods to detect the same synthetic *RecA* DNA (n=3). Fluorescent images obtained from the three loading methods did not show significant variations of digital PCR results. The reporter dye of *RecA* probe is FAM. Scale bar: 1 mm. (D) The detected DNA copies calculated from the three loading methods after correction using Poisson distribution show consistent results among the three loading methods.

3.5 Digital-PCR for Gram-positive bacterial single-cell detection

To further demonstrate the capability for running multi-step and multi-reagent assays on our device, we performed single-cell testing for a Gram-positive bacterium, Methicillin-resistant *S. aureus*. Enzymatic lysis, such as lysozyme and lysostaphin, are needed[22] to release nucleic acids from Gram-positive bacterial cells for molecular testing because of the stronger resistance to temperature or osmosis-induced cell lysis[23] caused by the hardy peptidoglycan layer in the cell

wall. However, enzymatic lysis is challenging on conventional microarray digital PCR platforms[24-26] as multiple loadings of reagents and dilution are necessary. Our multi-step loading device is an ideal solution for incorporating enzymatic lysis before PCR detection for single Gram-positive bacterial analysis. To do so, we first loaded 2 μL Methicillin-resistant *S. aureus* cell suspension into four chips, with expected bacteria numbers of 3000, 1500, 750, 375, and 100 CFU, respectively. Then, we loaded 2 μL of 4 μg/mL lysostaphin followed by incubation at 37 °C for 10 min to enable complete bacteria lysis. Finally, we filled the microchambers with PCR reaction mixture and digitized them using oil partitioning. After PCR amplification, chips were imaged and positive microchambers were counted (***Fig. 5A-E***). Three repetitive tests were performed for each concentration to ensure repeatability of results. A methicillin-sensitive *S. aureus* strain[27] (3000 CFU) was used as the negative control (***Fig. 5F***). We observed clear digital PCR amplifications in the chip with Methicillin-resistant *S. aureus* input while no fluorescent signal showed in the Methicillin-sensitive *S. aureus* control. Again, using the equation (1), the calculated cell number for each input concentration are 2279, 980, 545, 325, and 71 CFU, respectively, which represents a good linear relationship with the input bacteria concentration (R^2=0.9930) (***Fig. 5G***), suggesting quantification precision of the digital PCR performed on our multi-step loading devices. Collectively, we demonstrated that our multi-step loading allowed an additional simple and efficient enzymatic lysis of Gram-positive bacteria which was not possible in regular microarray designs and ultimately facilitated highly sensitive single-cell detection using digital PCR.

We noted the calculated cell numbers were lower than the expected values, which may be caused by a number of factors. Cell retention at the inlet or within the microchannel wall due to the surface roughness of PDMS chip[14], especially with small bacteria cells (0.5-1 μm in diameter), may contribute to the discrepancy. Furthermore, *Staphylococcal* spp. bacteria are often arranged in grape-like clusters during their cell division and it is difficult to resuspend all the bacteria into single cells, which can result in multiple cells being loaded into individual microchambers[27].

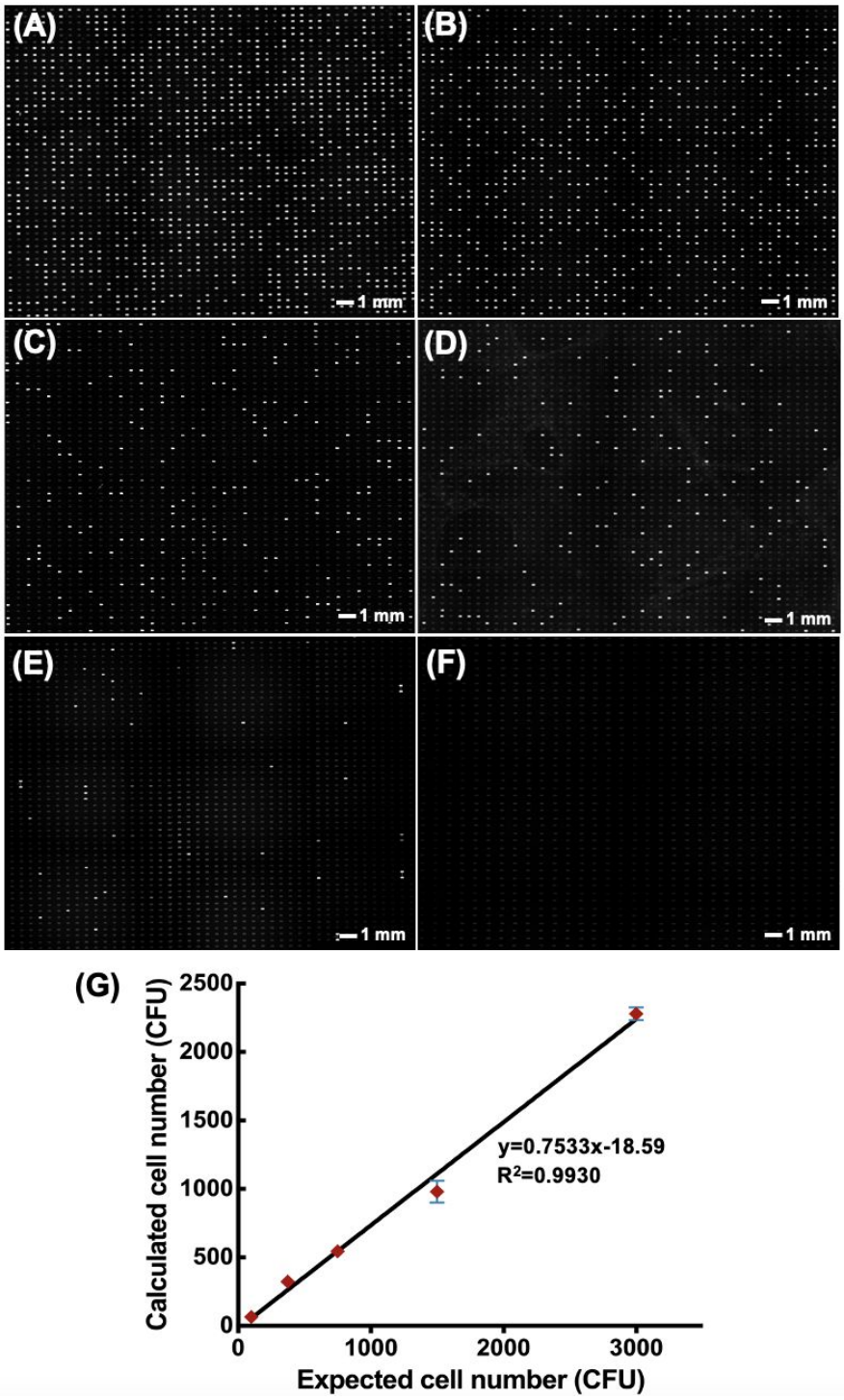

Fig. 5. Digital PCR quantification of Methicillin-resistant *S. aureus* on the multi-step loading devices. A single-cell suspension of Methicillin-resistant *S. aureus* was prepared and serially diluted using GW medium. Then 3000 (A), 1500 (B), 750 (C), 375 (D) and 100 CFU (E) of cells were tested on our device with three consecutive loading steps. As a negative control, 3000 CFU of Methicillin-sensitive *S. aureus* was tested using the same protocol (F). End-point single-cell digital PCR signals were detected using the ZEISS Axio Zoom V16 microscope. The reporter dye of *MecA* probe is HEX. Scale bar: 1 mm. (G) Linear regression curve was acquired by plotting the calculated number of cells after Poisson distribution against the expected number of cells. With high linearity of 0.9930, the difference between observed cell number and theoretical cell number is unbiased, showing accurate absolute quantification for *S. aureus* on our device.

4. Conclusions

We have developed a vacuum-assisted microarray device for multi-step and multi-reagent biological assays. Our device utilizes a suction layer connected to an external vacuum to provide continuous liquid driving force, and it features a microarray structure composed of the multi-level bifurcated microchannel and dead-end microchambers for liquid splitting. We adopted a unique thermosetting oil-poured glass coverslip onto the thin gas-permeable PDMS membrane to efficiently prevent evaporation during the thermocycling process. Using Fluorescein solution as a demonstration, we demonstrated the sample loading uniformity of our chip by analyzing the volume variations across microchambers. By comparing digital PCR amplification using multi-step versus single-step workflow, we showed the capacity of our device to perform single-molecule detection with multiple loading steps. Finally, we conducted single *Gram-positive bacteria* detection by incorporating an additional enzymatic lysis step that was otherwise hard to achieve in regular microarrays. This was done by loading single-cell suspension, lysis buffer, and PCR reaction mixture in separate steps. The highly correlated positive microchambers corroborated the efficient bacteria lysis using our multi-loading workflow that ultimately facilitated highly sensitive single-cell detection. Compared with reported platforms for multi-step loading, our device obviates complex control instrumentations and achieves high-throughput digital assay across 4096 microchambers. Furthermore, both the number of loading steps and the total number of microchambers can be further scaled up. Given that this device is highly flexible in performing various assays requiring multi-step and multi-reagent reactions as we usually do in benchtop, we envision that the application scope of our device can be greatly expanded to other fields such as enzymatic reactions[28] and immunoassays[29].

Acknowledgments

The authors are grateful for the financial support from the National Institutes of Health (R01AI137272 and R01AI138978) and the Defense Threats Reduction Agency (DTRA, MCDC-18-01-01-012).

References

1. M. Baker, *nature methods*, 2012, **9**, 541-544.
2. D. M. Rissin, C. W. Kan, T. G. Campbell, S. C. Howes, D. R. Fournier, L. Song, T. Piech, P. P. Patel, L. Chang, A. J. Rivnak, E. P. Ferrell, J. D. Randall, G. K. Provuncher, D. R. Walt and D. C. Duffy, *Nat Biotechnol*, 2010, **28**, 595-599.
3. B. J. Hindson, K. D. Ness, D. A. Masquelier, P. Belgrader, N. J. Heredia, A. J. Makarewicz, I. J. Bright, M. Y. Lucero, A. L. Hiddessen, T. C. Legler, T. K. Kitano, M. R. Hodel, J. F. Petersen, P. W. Wyatt, E. R. Steenblock, P. H. Shah, L. J. Bousse, C. B. Troup, J. C. Mellen, D. K. Wittmann, N. G. Erndt, T. H. Cauley, R. T. Koehler, A. P. So, S. Dube, K. A. Rose, L. Montesclaros, S. Wang, D. P. Stumbo, S. P. Hodges, S. Romine, F. P. Milanovich, H. E. White, J. F. Regan, G. A. Karlin-Neumann, C. M. Hindson, S. Saxonov and B. W. Colston, *Anal Chem*, 2011, **83**, 8604-8610.
4. C. M. Hindson, J. R. Chevillet, H. A. Briggs, E. N. Gallichotte, I. K. Ruf, B. J. Hindson, R. L. Vessella and M. Tewari, *Nat Methods*, 2013, **10**, 1003-1005.
5. K. A. Heyries, C. Tropini, M. Vaninsberghe, C. Doolin, O. I. Petriv, A. Singhal, K. Leung, C. B. Hughesman and C. L. Hansen, *Nat Methods*, 2011, **8**, 649-651.
6. E. A. Ottesen, J. W. Hong, S. R. Quake and J. R. Leadbetter, *science*, 2006, **314**, 1464-1467.

7. A. K. White, M. VanInsberghe, O. I. Petriv, M. Hamidi, D. Sikorski, M. A. Marra, J. Piret, S. Aparicio and C. L. Hansen, *Proceedings of the National Academy of Sciences*, 2011, **108**, 13999-14004.
8. D. V. Zhukov, E. M. Khorosheva, T. Khazaei, W. Du, D. A. Selck, A. A. Shishkin and R. F. Ismagilov, *Lab Chip*, 2019, **19**, 3200-3211.
9. Y. Zhu, Y. X. Zhang, W. W. Liu, Y. Ma, Q. Fang and B. Yao, *Sci Rep*, 2015, **5**, 9551.
10. L. Mazutis, J. C. Baret, P. Treacy, Y. Skhiri, A. F. Araghi, M. Ryckelynck, V. Taly and A. D. Griffiths, *Lab Chip*, 2009, **9**, 2902-2908.
11. R. M. Schoeman, E. W. Kemna, F. Wolbers and A. van den Berg, *Electrophoresis*, 2014, **35**, 385-392.
12. P. Shahi, S. C. Kim, J. R. Haliburton, Z. J. Gartner and A. R. Abate, *Sci Rep*, 2017, **7**, 44447.
13. Z. Dong and Q. Fang, *TrAC Trends in Analytical Chemistry*, 2020, **124**.
14. J. Hu, Y. Xu, T. Gou, S. Zhou and Y. Mu, *Analyst*, 2018, **143**, 5792-5798.
15. Q. Zhu, Y. Xu, L. Qiu, C. Ma, B. Yu, Q. Song, W. Jin, Q. Jin, J. Liu and Y. Mu, *Lab Chip*, 2017, **17**, 1655-1665.
16. J. M. Karlsson, M. Gazin, S. Laakso, T. Haraldsson, S. Malhotra-Kumar, M. Maki, H. Goossens and W. van der Wijngaart, *Lab Chip*, 2013, **13**, 4366-4373.
17. L. Xu, H. Lee, D. Jetta and K. W. Oh, *Lab Chip*, 2015, **15**, 3962-3979.
18. T. Xie, P. Wang, L. Wu, B. Sun, Q. Zhao and G. Li, *Lab on a Chip*, 2021.
19. C. M. O'Keefe, T. R. Pisanic, H. Zec, M. J. Overman, J. G. Herman and T.-H. Wang, *Science Advances*, 2018, **4**, eaat6459.
20. T. Gou, J. Hu, S. Zhou, W. Wu, W. Fang, J. Sun, Z. Hu, H. Shen and Y. Mu, *Analyst*, 2019, **144**, 3274-3281.
21. H. Ghaedamini, M. Salimpour and A. S. Mujumdar, *Applied Thermal Engineering*, 2011, **31**, 708-716.
22. M. Shehadul Islam, A. Aryasomayajula and P. Selvaganapathy, *Micromachines*, 2017, **8**.
23. M. Mahalanabis, H. Al-Muayad, M. D. Kulinski, D. Altman and C. M. Klapperich, *Lab Chip*, 2009, **9**, 2811-2817.
24. P. Athamanolap, K. Hsieh, C. M. O'Keefe, Y. Zhang, S. Yang and T. H. Wang, *Anal Chem*, 2019, **91**, 12784-12792.
25. C. M. O'Keefe, D. Giammanco, S. Li, T. R. Pisanic and T.-H. J. Wang, *Lab on a Chip*, 2019, **19**, 444-451.
26. K. Hsieh, H. C. Zec, L. Chen, A. M. Kaushik, K. E. Mach, J. C. Liao and T. H. Wang, *Anal Chem*, 2018, **90**, 9449-9456.
27. M. Schulz, S. Calabrese, F. Hausladen, H. Wurm, D. Drossart, K. Stock, A. M. Sobieraj, F. Eichenseher, M. J. Loessner, M. Schmelcher, A. Gerhardts, U. Goetz, M. Handel, A. Serr, G. Haecker, J. Li, M. Specht, P. Koch, M. Meyer, P. Tepper, R. Rother, M. Jehle, S. Wadle, R. Zengerle, F. von Stetten, N. Paust and N. Borst, *Lab Chip*, 2020, **20**, 2549-2561.
28. H. Li, E. Shkolyar, J. Wang, S. Conti, A. C. Pao, J. C. Liao, T. S. Wong and P. K. Wong, *Science Advances*, 2020, **6**.
29. H. Fu, P. Song, Q. Wu, C. Zhao, P. Pan, X. Li, N. Y. K. Li-Jessen and X. Liu, *Microsyst Nanoeng*, 2019, **5**, 50.